CHEMISTRY
A EUROPEAN JOURNAL

FULL PAPER

DOI: 10.1002/chem.201201414

Preparation of Photocatalytic Au–Ag_2Te Nanomaterials

Zong-Hong Lin, Zih-Yu Shih, Prathik Roy, and Huan-Tsung Chang*[a]

Abstract: A facile approach has been developed for the preparation of various morphologies of Au–Ag_2Te nanomaterials (NMs) that exhibit strong photocatalytic activity. Te NMs (nanowires, nanopencils, and nanorice) were prepared from TeO_2 in the presence of various concentrations (16, 8, and 4 M) of a reducing agent (N_2H_4) at different temperatures (25 and 60 °C). These three Te NMs were then used to prepare Au–Ag_2Te NMs by spontaneous redox reactions with Au^{3+} and Ag^+ ions sequentially. The Au–Ag_2Te nanopencils exhibit the highest activity toward degradation of methylene blue and formation of active hydroxyl radicals on solar irradiation, mainly because they absorb light in the visible region most strongly. All three differently shaped Au–Ag_2Te NMs (10 μg mL^{-1}) provide a death rate of *Escherichia coli* greater than 80 % within 60 min, which is higher than that of 51 % for commercial TiO_2 nanoparticles (100 μg mL^{-1}). Under light irradiation, the Au NPs in Au–Ag_2Te NMs enhance the overall photo-oxidation ability of Ag_2Te NMs through faster charge separation because of good contact between Ag_2Te and Au segments. With high antibacterial activity and low toxicity toward normal cells, the Au–Ag_2Te NMs hold great potential for use as efficient antibacterial agents.

Keywords: antibiotics · nanostructures · photocatalysis · silver · tellurium

Introduction

Pathogenic bacteria that cause a large number of diseases and high death rate each year remain a major health concern.[1] For example, *Escherichia coli* (*E. coli*) existing in cucumbers caused the death of at least 50 people in Europe,[2] and also increased concerns about food safety. Although numerous antibacterial agents have been synthesized and even commercialized,[3] they tend to be expensive, unstable, too specific, and/or toxic. Thus, cheap and environmentally friendly agents that allow effective killing of common bacteria such as *E. coli* and *Staphylococcus aureus* are still urgently required.

Antibacterial agents are either organic or inorganic compounds. Compared to organic antibacterial reagents, inorganic reagents such as metal oxides are robust and durable, and have become more popular in recent years.[4] Metal oxide nanoparticles (NPs) such as titanium dioxide (TiO_2), silicon dioxide (SiO_2), and zinc oxide (ZnO) display strong biocidal activity against both Gram-positive and Gram-negative bacteria.[5] These NPs have a relatively large surface area and can generate reactive oxygen species (ROS) under high-intensity light at a specific wavelength. Among them, only TiO_2 NPs exhibit antibacterial activity under sunlight illumination. Unfortunately, the antibacterial activity of pure TiO_2 NPs is marginal. In addition, the photocatalytic sterilization of TiO_2 NPs is highly restricted, mainly because of a low electron transfer rate to oxygen adsorbed on their surfaces and a high electron–hole recombination rate.[6] These drawbacks greatly restrict the practical application of TiO_2 NPs as antibacterial agents.

Various Ag nanomaterials (NMs) have been demonstrated to have antibacterial properties with the major advantage of outstanding broad-spectrum antimicrobial activity.[7] Although Ag NMs are effective, they are reportedly toxic to zebra fish,[8] *Drosophila melanogaster*,[9] and mammalian cell lines of mice,[10] rats,[11] and humans.[12] Ag–TiO_2[13] and Ag–Ag_2S[14] were recently synthesized and used as antibacterial agents. Relative to pure Ag NMs, Ag–TiO_2 NMs are cheaper and can be used under harsher conditions (e.g., high salt concentration or high pH), while Ag–Ag_2S NMs are more stable under prolonged UV irradiation. However, because a long irradiation time (3 h) and a large volume (100 μg mL^{-1}) are required when using Ag–TiO_2 and Ag–Ag_2S NMs, respectively, these NMs are still not completely effective. In addition, the antibacterial activities of Ag–TiO_2 and Ag–Ag_2S NMs are mainly generated under irradiation in the UV region.

We have now developed a facile approach for the preparation of a new antibacterial agent, namely, Au–Ag_2Te NMs (β type). The monoclinic structure of Ag_2Te (β-Ag_2Te) has a narrow bandgap with high electron mobility and low lattice thermal conductivity.[15,16] On the other hand, Au serves as a sink for electrons and a redox catalyst that may enhance the overall photo-oxidation ability of the new material.[17] We prepared Au–Ag_2Te nanowires, nanopencils, and nanorice

---

[a] Dr. Z.-H. Lin, Z.-Y. Shih, P. Roy, Prof. H.-T. Chang
Department of Chemistry
National Taiwan University
1, Section 4, Roosevelt Road, Taipei 106 (Taiwan)
Fax: (+886) 2-33661171
E-mail: changht@ntu.edu.tw

Supporting information for this article is available on the WWW under http://dx.doi.org/10.1002/chem.201201414.

by controlling the concentration of the reducing agent (N_2H_4) and the reaction temperature ($\leq 60\,°C$). The antibiotic activity of the as-prepared Au–Ag_2Te NMs against *E. coli* was investigated. The antibacterial properties of Au–Ag_2Te NMs result from the Ag^+ ions released and ROS generated from Ag_2Te under light irradiation.

Results and Discussion

Synthesis of Au–Ag_2Te NMs: Te nanowires with a width of 20 ± 3 nm and a length of 880 ± 170 nm were synthesized in the presence of 16 M N_2H_4 at 25 °C.[18] Te nanopencils having a width of 70 ± 10 nm and a length of 440 ± 70 nm were prepared in the presence of 8 M N_2H_4 at 60 °C. Te nanorice having a width of 50 ± 8 nm and a length of 130 ± 20 nm was prepared in the presence of 4 M N_2H_4 at 60 °C. The three differently shaped Te NMs were used to prepare the corresponding Au–Te NMs through a redox reaction between Au^{3+} ions and Te atoms in Te NMs.[19,20] Figure 1 A–C display TEM images of Au–Te nanowires, nanopencils, and nanorice, respectively. In addition, some Au NPs are visible on their surfaces (dark parts). The as-prepared Au–Te NMs had similar structures to their corresponding Te NMs. The Au–Te nanowires, nanopencils, and nanorice were further used to prepare Au–Ag_2Te NMs through a redox reaction between Te atoms and Ag^+ ions.[21] Figure 1 D–F display their respective TEM images. Au–Ag_2Te NMs had similar structures to their corresponding Au–Te NMs but with rough surfaces. The average widths of Au–Ag_2Te nanowires, nanopencils, and nanorice of 25, 80, and 55 nm, respectively, are larger than those of Au–Te nanowires (20 nm), nanopencils (70 nm), and nanorice (50 nm). In addition, the existence of Au NPs on the surfaces became more apparent. The morphology preservation of Ag_2Te NMs is similar to the transformation of Se NMs into Ag_2Se NMs.[22]

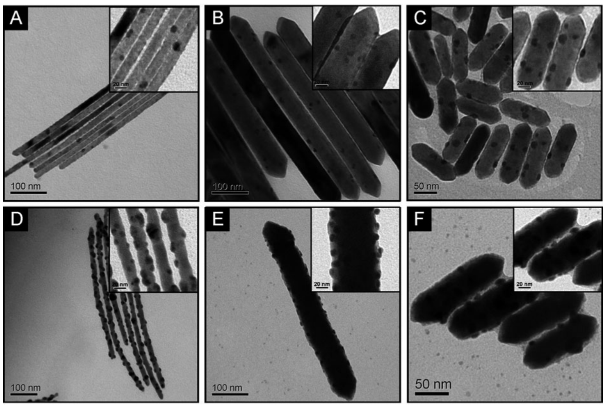

Figure 1. TEM images of NMs. Au–Te nanowires (A), nanopencils (B), and nanorice (C) and Au–Ag_2Te nanowires (D), nanopencils (E), and nanorice (F). Insets are enlarged TEM images of the NMs.

Figure 2 A shows an HRTEM image of a representative Au–Ag_2Te nanowire. The interplanar spacing of 0.23 nm corresponds to the (111) lattice planes of the Au structure, and that of 0.28 nm to the (220) lattice plane of the Ag_2Te structure. Unlike Au–CdS,[23] Au–CdSe,[24] Au–CdTe,[25] Au–PbS,[26] Au–PbSe,[27] and Au–Ag_2S[28] prepared in organic solutions, the Au–Ag_2Te NMs were prepared in an aqueous solution. In addition, our rapid and simple approach allows large-scale preparation of Au–Ag_2Te NMs. Energy dispersive X-ray (EDX) analysis of Au–Ag_2Te nanowires (Supporting Information Figure S1) revealed that the Ag/Te atomic ratio was 2/1 in all Au–Ag_2Te NMs. Elemental mapping images of Ag, Te, and Au on a single Au–Ag_2Te nanowire (Figure 2 C–F) obtained by high-angle annular dark-field STEM energy-dispersive X-ray (HAADF-STEM-EDX) spectroscopy revealed that Ag and Te were uniformly dispersed on the nanowire and Au NPs were formed on its surface. The ICP-MS data revealed that the weight percentages of Au in the as-prepared Au–Ag_2Te nanowires, nanopencils, and nanorice were 2.5, 2.9, and 2.2 %. respectively. The absorption spectra of the three Au–Ag_2Te NMs (Supporting Information Figure S2) are similar to those of Ag_2Te NMs.[29] All spectra exhibit a broad absorption band centered around 410 nm with a small shoulder at approximately 530 nm ascribed to the surface plasmon resonance (SPR) of Au NPs. The weak SPR observed here is due to the small size of the Au NPs (< 10 nm) and their small amount compared to Ag_2Te NMs. The other reason for weak SPR is good contact between Ag_2Te and Au, which ensures effective charge transfer across the phase boundary.[30] To understand charge transfer within the Au–Ag_2Te system, simplified band structures of the two materials before and after contact are depicted in Figure S3 of the Supporting Informa-

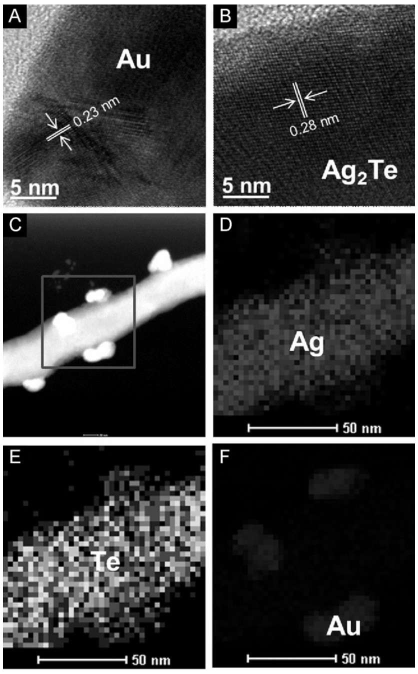

Figure 2. A, B) HRTEM images and C)–F) HAADF-STEM-EDX mapping images of a typical Au–Ag_2Te nanowire.

tion. On contact, the electrons (majority carriers) flow from the Fermi level of Au to the Fermi level of Ag_2Te, leaving some positive charge buildup on the metal contact interface. The electrons in the conduction band of Ag_2Te move to the Au side more easily, due to the attraction of the opposite charge buildup (see the downward band bending and carrier accumulation layer X_A in Supporting Information Figure S3B), whereas the holes in the valence band experience an energy barrier to traveling to the metal side. There are two major photon-promoted electron transitions in Ag_2Te, from the valence band to the bottom energy level and to the dominant energy level within the conduction band.

Powder XRD data revealed the presence of Au NPs and Ag_2Te NMs in Au–Ag_2Te NMs (Figure 3). The characteristic crystal facets for Au at (111), (200), (220), and (311) are also apparent in the XRD patterns. The (220), (032), (123), (202), (320), (301), and (103) crystal facets reveal a monoclinic phase of Ag_2Te in Au–Ag_2Te NMs. The chemical composition of the Au–Ag_2Te NMs was further confirmed by X-ray photoelectron spectroscopy (XPS, Figure 4), which revealed the existence of Ag, Te, and Au in the Au–Ag_2Te nanowires. The peaks at 368.1 and 572.0 eV correspond to Ag $3d_{5/2}$ and Te $3d_{5/2}$, respectively, revealing the existence of Ag (+1) and Te (−2) valence states. The peaks at 368.3 and 374.1 eV correspond to $Ag3d_{5/2}$ and $Ag3d_{3/2}$, respectively (Figure 4A), and those at 572.5 and 582.4 eV to $Te3d_{5/2}$ and $Te3d_{3/2}$ (Figure 4B), respectively. Two small peaks at 575.6 and 586.0 eV are attributed to Te^{IV} oxide.[29] The peaks at 83.7 and 87.4 eV correspond to $Au4f_{7/2}$ and $Au4f_{5/2}$ (Figure 4C), respectively, with slight shifts due to the presence of the Ag component. The observed shifts in the Au–Ag_2Te nanowires indeed closely match those of the Au–Ag bimetallic NMs.[31]

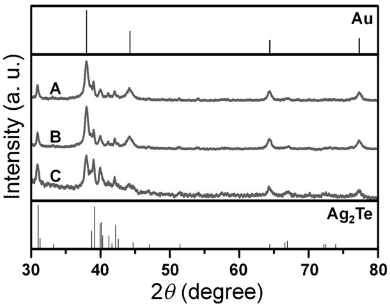

Figure 3. XRD spectra of Au–Ag_2Te nanowires (A), nanopencils (B), and nanorice (C).

Photocatalytic activity of Au–Ag_2Te NMs: Ag_2Te is an n-type semiconductor. When the Ag_2Te NMs are activated by light irradiation with photon energies that matched or exceeded the bandgap energy E_g (a wavelength which matched or was shorter than the absorption edge for Ag_2Te), pairs of conduction-band electrons (e^-) and valence-band holes (h^+) are generated at the surface of Ag_2Te NMs [Eq. (1)].

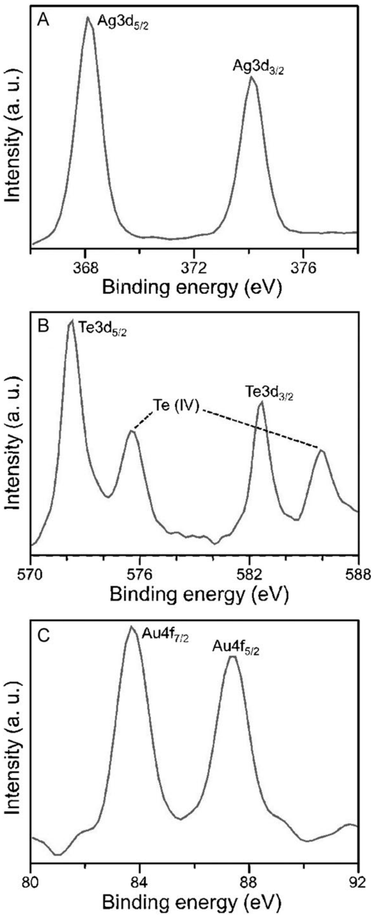

Figure 4. XPS spectra of Ag_{3d} (A), Te_{3d} (B), and Au_{4f} (C) regions of the Au–Ag_2Te nanowires.

$$2\,Ag_2Te + h\nu \rightarrow Ag_2Te\ (e^-) + Ag_2Te\ (h^+) \qquad (1)$$

Holes react with water adsorbed on the surface of semiconductor Ag_2Te to generate highly reactive hydroxyl radicals ($^{\bullet}OH$), while O_2 acts as an electron acceptor to generate a superoxide radical anion ($O_2^{\bullet -}$), which can act as oxidizing agent or as an additional source of $^{\bullet}OH$ [Eqs. (2)–(4)].

$$H_2O + Ag_2Te\ (h^+) \rightarrow {}^{\bullet}OH + H^+ + Ag_2Te \qquad (2)$$

$$O_2 + Ag_2Te\ (e^-) \rightarrow O_2^{\bullet -} + Ag_2Te \qquad (3)$$

$$O_2^{\bullet -} + H^+ \rightarrow {}^{\bullet}OOH \qquad (4)$$

These radicals have strong oxidizing ability and can degrade methylene blue [MB, Eq. (5)].[32–34]

$$MB + O_2/O_2^{\bullet -}/{}^{\bullet}OH/{}^{\bullet}OOH \rightarrow \text{degradation products} \qquad (5)$$

Figure 5A shows the changes in the absorption spectra of an MB solution exposed to solar light for various reaction times in the presence of Ag_2Te nanopencils. MB, a typical dye for photodegradation, was used as the test pollutant to monitor the photocatalytic progress.[35] Under solar irradia-

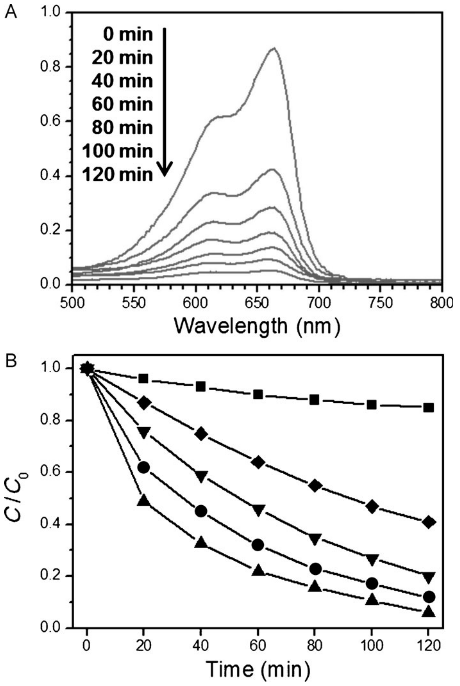

Figure 5. A) Changes in the UV/Vis absorption of MB aqueous solution under light irradiation in the presence of Au–Ag_2Te nanopencils. B) Comparison of photocatalytic activity of the Au–Ag_2Te nanowires (▼), nanopencils (▲), nanorice (●), TiO_2 NPs (◆), and a control (■).

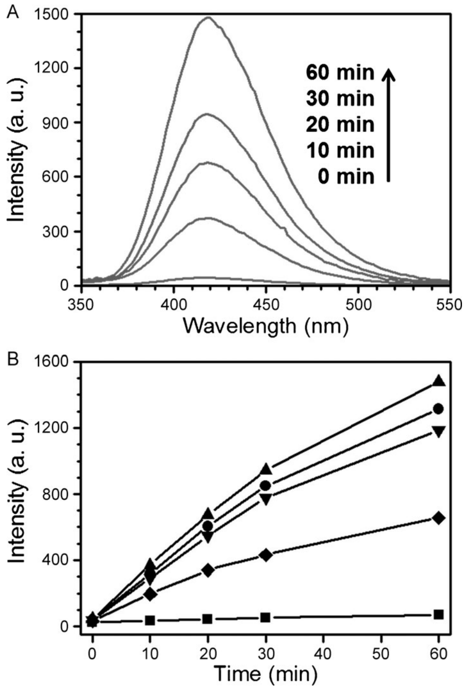

Figure 6. A) Changes in the fluorescence of TA solution under light irradiation in the presence of Au–Ag_2Te nanopencils. B) Comparison of photocatalytic activity of the Au–Ag_2Te nanowires (▼), nanopencils (▲), nanorice (●), TiO_2NPs (◆), and a control (■).

tion, the absorbance at 662 nm drops rapidly due to rapid decomposition of MB. The blue color of the solution almost disappeared after 120 min of irradiation. Figure 5B shows slight degradation of MB in the absence of any photocatalyst (control experiment), that is, the extent of self-photolysis of MB under solar irradiation is small.[36] Since the absorbance of the solution did not change in the dark, light is needed for MB decomposition. Under light irradiation, the decreasing order of MB photodegradation is Au–Ag_2Te nanopencils > Au–Ag_2Te nanorice > Au–Ag_2Te nanowires > TiO_2 NPs (Figure 5B). After 120 min, the C/C_0 values were 0.41, 0.20, 0.12, and 0.06 in the presence of TiO_2 NPs, Au–Ag_2Te nanowires, nanorice, and nanopencils, respectively, where C and C_0 are the concentrations of MB at reaction times t and 0, respectively. The broader absorption band of Au–Ag_2Te nanopencils in the visible region reveals that the charge-separation efficiency likely played some role in increasing their photocatalytic activity. All three Au–Ag_2Te NMs provided photodegradation efficiencies of MB greater than 80 % within 120 min. After five recycles of the Au–Ag_2Te nanopencils, no significant loss of their activity was observed (Supporting Information Figure S4), that is, its high stability during the photocatalytic degradation of MB is high.

The photocatalytic activity of the as-prepared Au–Ag_2Te NMs was further confirmed by measuring the formation of active $^{\bullet}$OH on irradiation, which is considered to be the most important oxidative species in photocatalytic reactions.[37] Figure 6A displays the fluorescence spectra of terephthalic acid (TA) solution in the presence of Au–Ag_2Te nanopencils under solar irradiation in solution. A gradual increase in the fluorescence intensity at 418 nm was observed. On the other hand, the fluorescence intensity did not increase in the absence of solar irradiation or photocatalyst. Figure 6B compares the as-prepared Au–Ag_2Te NMs and TiO_2 NPs in the photocatalytic reaction of TA to give a fluorescent product. The fluorescence intensity is proportional to the amount of produced $^{\bullet}$OH.[38] At a fixed time (60 min), the amount of $^{\bullet}$OH generated from Au–Ag_2Te nanopencils is larger than those from TiO_2 NPs, Au–Ag_2Te nanowires, and Au–Ag_2Te nanorice. The results again confirm that the Au–Ag_2Te nanopencils have the highest photocatalytic activity among the as-prepared Au–Ag_2Te NMs. The photocatalytic activity of Au–Ag_2Te nanopencils is 2.3 times higher than that of commercial TiO_2 NPs.

Antibacterial properties of Au–Ag_2Te NMs: The antibacterial properties of the as-prepared Au–Ag_2Te NMs and TiO_2 NPs against *E. coli* were assessed. These three Au–Ag_2Te NMs were stable for at least one week in LB medium (Supporting Information Figure S5). Representative micrographs of *E. coli* incubated in LB medium with and without Au–Ag_2Te nanowires, nanopencils, and nanorice under light irradiation for 60 min are depicted in Figure 7. The green and red images correspond to live and dead *E. coli*, respectively. Without light irradiation (Figure 8A), the decreasing order of the viability of *E. coli* in the presence of various NMs is Au–Ag_2Te nanorice > Au–Ag_2Te nanowires > Au–Ag_2Te

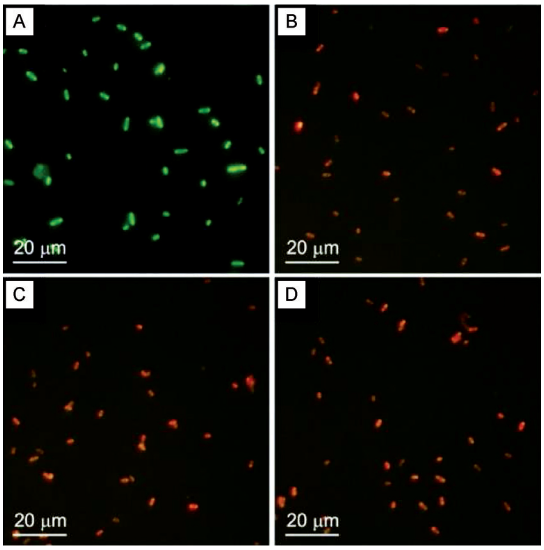

Figure 7. Fluorescence images of *E. coli* in LB medium under light irradiation for 60 min without NMs (A) and with Au–Ag_2Te nanowires (B), nanopencils (C), and nanorice (D). *E. coli.* cells were stained with SYTO 9/PI. Green and red fluorescent stains are representatives of live and dead (or compromised) cells, respectively.

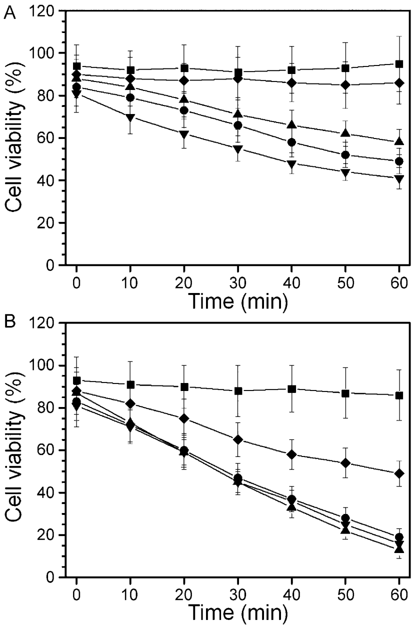

Figure 8. Cell viability of *E. coli* in LB media without (A) and with solar irradiation for 60 min (B). Cells were mixed with Au–Ag_2Te nanowires (●), nanopencils (▲), nanorice (▼), and TiO_2 NPs (◆) during irradiation. Control (■): cells were not treated with NMs.

nanopencils > TiO_2 NPs. After 60 min, the viabilities were 86, 58, 49, and 41 % in the presence of TiO_2 NPs (100 $\mu g mL^{-1}$) and Au–Ag_2Te nanopencils, nanowires, and nanorice (all 10 $\mu g mL^{-1}$), respectively. Under light irradiation, the decreasing order of the viability of *E. coli* is Au–Ag_2Te nanopencils > Au–Ag_2Te nanorice > Au–Ag_2Te nanowires > TiO_2 NPs (Figure 8B). After 60 min, the viabilities were 49, 19, 16, and 13 % in the presence of TiO_2 NPs (100 $\mu g mL^{-1}$) and Au–Ag_2Te nanowires, nanorice, and nanopencils, respectively. All three Au–Ag_2Te NMs provided a death rate of *E. coli* that was greater than 80 %.

To understand the antibacterial activities of Au–Ag_2Te NMs against *E. coli*, the ions released from these NMs at different times with or without light irradiation were investigated (Supporting Information Figure S6). The ICP-MS data reveal that the concentrations of the released TeO_3^{2-} and Ag ions were up to 0.25 and 0.01 $\mu g mL^{-1}$, respectively, once the NMs were added separately to the cell media. The concentrations of TeO_3^{2-} ions in the media decreased gradually over 0–60 min, while the Ag^+ ion concentration remained almost constant. We suspected that the presence of chloride ions in the cell media led to formation of $AgCl_{(s)}$ with the dissolved Ag^+ ions. This was supported by the higher concentrations of Ag^+ ions when Au–Ag_2Te NMs were prepared in ultrapure water. Although both Ag and TeO_3^{2-} ions exhibit strong antibacterial activities, Ag ions become less bioavailable in the presence of chloride ions because the solubility of AgCl is very low.[39] Thus, the antibacterial activities of Au–Ag_2Te NMs were mainly because of the released TeO_3^{2-} ions. TeO_3^{2-} ions are toxic to most microorganisms, particularly Gram-negative bacteria,[40] mainly because of their strong oxidant nature.[41] A representative TEM image (Supporting Information Figure S7) shows that many Te NPs (35 nm in diameter) were formed inside *E. coli* after treatment with Au–Ag_2Te nanowires. The Te NPs are formed through reduction of TeO_3^{2-} ions in the presence of reducing agents including glutathione, cysteine, and other reducing thiol-containing compounds in the cell media and/or inside the cell.[42] We note that similar Te NPs were formed inside *E. coli* after treatment with the other two shapes of Au–Ag_2Te NMs. The decreasing order of the released TeO_3^{2-} ions from Au–Ag_2Te NMs is nanorice > nanowires > nanopencils, which is consistent with the result of the antibacterial tests in the dark. The results reveal that the formation of TeO_3^{2-} ions is mainly responsible for the antibacterial activity of Au–Ag_2Te NMs in the dark. Compared with those conducted in the dark, stronger antibacterial activity of these NMs under solar light irradiation was achieved; however, the concentrations of the released TeO_3^{2-} and Ag^+ ions were almost the same. Similar concentrations of the released ions suggest that stronger antibacterial activity under light irradiation is due to the production of ROS.[43,44] As shown in Figure S2 (Supporting Information), a broader absorption band (530 nm) of Au–Ag_2Te nanopencils reveals that heat likely played some role in increasing their antibacterial activity and determining the order of antibacterial activity among the three Au–Ag_2Te NMs.

To verify the bactericidal role played by Au and Ag_2Te in Au–Ag_2Te NMs, we also tested the antibacterial activities of Au–Te and Ag_2Te NMs. Without light irradiation, the viabilities of *E. coli* were 53, 63, and 46 % in the presence of Au–Te nanowires, nanopencils, and nanorice, respectively. Although Au–Te NMs exhibit comparable antibacterial activities to Au–Ag_2Te NMs in the dark, no enhancement of antibacterial activity was observed under light illumination. Alternatively, under light illumination for 60 min, the viabilities of *E. coli* were 37, 28, and 31 in the presence of Ag_2Te nanowires, nanopencils, and nanorice, respectively. These results support that Au NPs in Au–Ag_2Te NMs enhanced the overall photo-oxidation ability of Ag_2Te NMs because of a more rapid charge separation.[45–48] It is important to verify the safety of using Au–Ag_2Te NMs as an antibacterial agent. We compared the toxicity of Au–Ag_2Te NMs and TiO_2 NPs in LLC-PK1 cells (Supporting Information Figure S8). This revealed that Au–Ag_2Te NMs have low toxicity, was comparable with that of TiO_2 NPs, mainly because of their stability inside the cells and in the cell media.

Conclusion

Three differently shaped Au–Ag_2Te NMs were prepared and tested as effective antibacterial agents against *E. coli*. These three high-quality Au–Ag_2Te NMs were readily prepared through spontaneous redox reactions of Te NMs with Au^{3+} and Ag^+ ions sequentially. The antibacterial activities of these three Au–Ag_2Te NMs against *E. coli* are high. Relative to Au–Ag_2Te nanowires, nanorice, and TiO_2 NPs, Au–Ag_2Te nanopencils with a broad absorption band in the visible region exhibited stronger antibacterial activity. In the dark, the formation of TeO_3^{2-} ions is responsible for the biocidal action. Under light irradiation, the production of ROS further enhances the antibacterial activity of Au–Ag_2Te NMs. The low toxicity of Au–Ag_2Te NMs against mammalian cells (LLC-PK1) is similar to that of TiO_2 NPs. Considering their strong antibacterial activity and low toxicity against normal cells, Au–Ag_2Te NMs have high potential as effective antibacterial reagents.

Experimental Section

Synthesis of Te NMs: Differently shaped Te NMs (nanowires, nanopencils, and nanorice) were prepared by reduction of TeO_2 with N_2H_4 under different conditions. In general, Te nanowires were prepared by slowly adding N_2H_4 (16 M, 10 mL) to a beaker containing TeO_2 powder (16 mg) over 2 h at an ambient temperature of 25 °C under constant magnetic stirring. For the preparation of other shapes of Te NMs, TeO_2 powder (16 mg) was dissolved in NaOH solution (20 mM, 1 mL) to form soluble TeO_3^{2-} ions. Then, 5 and 2.5 mL of N_2H_4 (final concentrations: 8 and 4 M) were added to synthesize Te nanopencils and nanorice, respectively. The mixtures were heated at 60 °C for 2 h and the total volumes of the solutions were 10 mL. To terminate the reactions and stabilize the as-prepared Te NMs, the mixtures were diluted to 100 mL with 10 mM sodium dodecyl sulfate (SDS). Each of the as-prepared Te NMs was subjected to a centrifugation/wash cycle to remove most of the matrices including SDS and N_2H_4.

Growth of Au NPs on Te NMs: Through a redox reaction between Au^{3+} ions and Te NMs, Au NPs were formed on the surfaces of Te NMs, while TeO_3^{2-} ions were released into the bulk solution. In a typical synthesis, Te NMs were redispersed in a cetyltrimethylammonium bromide (CTAB) solution (10 mM); after 10 min, various volumes of 0.1 M HCl were separately added to the mixtures to adjust their pH to 7.0. After 1 min, aqueous $NaAuCl_4$ (10 mM, 200 μL) was added to each solution and the mixture maintained at an ambient temperature of 25 °C for 10 min to allow the growth of Au NPs on the surfaces of Te NMs.

Preparation of Au–Ag_2Te NMs: Aqueous $AgNO_3$ (final concentration: 1 mM) was added to each of the as-prepared aqueous solutions of Au-Te NMs. The mixtures were kept at an ambient temperature of 25 °C for 3 h and was then subjected to three centrifugation/wash cycles to remove most of the matrices. Centrifugation was conducted at 15000 rpm for 10 min and ultrapure water (100 mL × 3) was used to wash the pellets (Au–Ag_2Te NMs). The pellets were dried in air at an ambient temperature of 25 °C prior to characterization and antibacterial tests.

Photocatalytic activity: The photocatalytic activities of Au–Ag_2Te NMs for photodegradation of methylene blue (MB) and formation of hydroxyl radicals (•OH) at ambient temperature under solar irradiation (intensity 100 mW/cm^2) and in the dark were evaluated separately. For comparison, as-prepared Au–Ag_2Te NMs (nanowires, nanopencils, and nanorice) and TiO_2 NPs were used. In a typical experiment, each of the photocatalysts (10 mg) was added to MB solution (20 μM, 20 mL). Prior to irradiation, each mixture was stirred in the dark for 30 min to reach the adsorption–desorption equilibrium between the photocatalyst and MB. At certain time intervals (every 20 min) of irradiation, aliquots of the mixtures were withdrawn (1.0 mL) and centrifuged to remove the photocatalyst. The absorbance values at 662 nm of the supernatants were recorded with a UV/Vis spectrophotometer. Reusability and stability of the Au–Ag_2Te nanopencils were studied through five cycles of photocatalytic reactions. In a typical experiment on formation of •OH radicals, each of the photocatalysts (10 mg) was added to terephthalic acid (TA) solution (3.0 mM, 20 mL) containing NaOH (10 mM). Prior to irradiation, the reaction solution was stirred in the dark for 30 min to reach adsorption–desorption equilibrium between the photocatalyst and TA. At certain time intervals (every 10 min) of irradiation, aliquots (1.0 mL) of the mixtures were withdrawn and centrifuged to remove the photocatalyst. The fluorescence values at 418 nm (excitation wavelength 320 nm) of the supernatants were recorded by using a fluorescence microplate reader. TA and •OH reacted to produce fluorescent 2-hydroxyterephthalic acid (TAOH) in the presence of the photocatalysts during photocatalysis.

Antibacterial tests: *E. coli* DH5α was grown in sterile LB medium, which was prepared by dissolving Bacto Tryptone (2.5 g), Bacto Yeast Extract (1.25 g), and NaCl (2.5 g) in H_2O (250 mL) and then adjusted to pH 7.0 by adding certain volumes of NaOH (5.0 M). A single colony of each strain was lifted from an LB agar plate and inoculated in LB medium (10 mL). The culture was then grown overnight until the absorbance at 600 nm wavelength (A_{600}) reached 1.0. A portion of each of the cell mixtures (1 mL) was centrifuged (4000 rpm, 10 min) and washed three times with 0.85 % NaCl to remove the matrix. Cells diluted to 4.0×10^8 CFU mL^{-1} were incubated in LB medium with and without being treated with Au–Ag_2Te NMs (10 μg mL^{-1}), Au–Te NMs, Ag_2Te NMs, or TiO_2 NPs (100 μg mL^{-1}). These cells were either subjected to solar irradiation (intensity 100 mW cm^{-2}) for 60 min or kept in the dark. The viability assay was conducted with SYTO 9 (6 μM) and propidium iodide (PI; 30 μM) stains. Each of the cell samples treated with Au–Ag_2Te NMs, Au–Te NMs, Ag_2Te NMs, or TiO_2 NPs was then subjected to three centrifugation/wash cycles [centrifugation at 4000 rpm for 10 min, wash with 0.85 % NaCl (3 × 1 mL)] to remove the matrix. Each of the bacterial suspensions (100 μL) was dispensed in a 96-well plate, and then the dye mixture (100 μL) was added to each well. The mixtures were incubated for 15 min at an ambient temperature of 25 °C. Fluorescence intensities of SYTO 9 (green; excitation wavelength: 475 nm, emission wavelength: 530 nm) and PI (red; excitation wavelength: 475 nm, emission wavelength: 640 nm) were recorded. The green/red fluorescence intensity ratio was used to calculate the percentage of live/dead cells.

Acknowledgements

This study was supported by the National Science Council of Taiwan under the contract NSC 98-2113M-002-011-MY3.

---

[1] N. Musee, M. Thwala, N. Nota, *J. Environ. Monit.* **2011**, *13*, 1164.
[2] D. A. Rasko, D. R. Webster, J. W. Sahl, A. Bashir, N. Boisen, F. Scheutz, E. E. Paxinos, R. Sebra, C. S. Chin, D. Iliopoulos, A. Klammer, P. Peluso, L. Lee, A. O. Kislyuk, J. Bullard, A. Kasarskis, S. Wang, J. Eid, D. Rank, J. C. Redman, S. R. Steyert, J. Frimodt-Møller, C. Struve, A. M. Petersen, K. A. Krogfelt, J. P. Nataro, E. E. Schadt, M. K. Waldor, *N. Engl. J. Med.* **2011**, *365*, 709.
[3] A. F. Stepan, D. P. Walker, J. Bauman, D. A. Price, T. A. Baillie, A. S. Kalgutkar, M. D. Aleo, *Chem. Res. Toxicol.* **2011**, *24*, 1345.
[4] L. K. Adams, D. Y. Lyon, P. J. Alvarez, *Water Res.* **2006**, *40*, 3527.
[5] W. Jiang, H. Mashayekhi, B. Xing, *Environ. Pollut.* **2009**, *157*, 1619.
[6] K. Page, M. Wilson, I. P. Parkin, *J. Mater. Chem.* **2009**, *19*, 3819.
[7] M. Rai, A. Yadav, A. Gade, *Biotechnol. Adv.* **2009**, *27*, 76.
[8] P. Asharani, Y. Wu, Z. Gong, S. Valiyaveettil, *Nanotechnology* **2008**, *19*, 255102.
[9] M. Ahamed, R. Posgai, T. J. Gorey, M. Nielsen, S. M. Hussain, J. J. Rowe, *Toxicol. Appl. Pharmacol.* **2010**, *242*, 263.
[10] L. Braydich-Stolle, S. Hussain, J. Schlager, M. Hofmann, *Toxicol. Sci.* **2005**, *88*, 412.
[11] S. Hussain, K. Hess, J. Gearhart, K. Geiss, J. Schlager, *Toxicol. in Vitro* **2005**, *19*, 975.
[12] P. V. Asharani, G. L. K. Mun, M. P. Hande, S. Valiyaveettil, *ACS Nano* **2009**, *3*, 279.
[13] Q. Xiang, J. G. Yu, B. Cheng, H. C. Ong, *Chem. Asian J.* **2010**, *5*, 1466.
[14] M. Pang, J. Hu, H. C. Zeng, *J. Am. Chem. Soc.* **2010**, *132*, 10771.
[15] A. Husmann, J. B. Betts, G. S. Boebinger, A. Migliori, T. F. Rosenbaum, T. F. Saboungi, *Nature* **2002**, *417*, 421.
[16] J. J. Urban, D. V. Talapin, E. V. Shevchenko, C. R. Kagan, C. B. Murray, *Nat. Mater.* **2007**, *6*, 115.
[17] M. Es-Souni, H. Fischer-Brandies, M. Es-Souni, *Adv. Funct. Mater.* **2008**, *18*, 3179.
[18] Z.-H. Lin, Z. Yang, H.-T. Chang, *Cryst. Growth Des.* **2008**, *8*, 351.
[19] Z.-H. Lin, Y.-W. Lin, K.-H. Lee, H.-T. Chang, *J. Mater. Chem.* **2008**, *18*, 2569.
[20] Z.-H. Lin, H.-T. Chang, *Langmuir* **2008**, *24*, 365.
[21] G. D. Moon, S. Ko, Y. Xia, U. Jeong, *ACS Nano* **2010**, *4*, 2307.
[22] U. Jeong, Y. Xia, *Angew. Chem.* **2005**, *117*, 3159; *Angew. Chem. Int. Ed.* **2005**, *44*, 3099.
[23] L. Carbone, S. Kudera, C. Giannini, G. Ciccarella, R. Cingolani, P. D. Cozzoli, L. Manna, *J. Mater. Chem.* **2006**, *16*, 3952.
[24] J. T. Zhang, Y. Tang, K. Lee, M. Ouyang, *Nature* **2010**, *466*, 91.
[25] J. Lee, P. Hernandez, J. Lee, A. O. Govorov, N. A. Kotov, *Nat. Mater.* **2007**, *6*, 291.
[26] J. Yang, H. I. Elim, Q. Zhang, J. Y. Lee, W. Ji, *J. Am. Chem. Soc.* **2006**, *128*, 11921.
[27] W. L. Shi, H. Zeng, Y. Sahoo, T. Y. Ohulchanskyy, Y. Ding, Z. L. Wang, M. Swihart, P. N. Prasad, *Nano Lett.* **2006**, *6*, 875.
[28] J. Yang, J. Y. Ying, *Chem. Commun.* **2009**, 3187.
[29] A. K. Samal, T. Pradeep, *J. Phys. Chem. C* **2009**, *113*, 13539.
[30] R. Costi, A. E. Saunders, E. Elmalem, A. Salant, U. Banin, *Nano Lett.* **2008**, *8*, 637.
[31] C.-C. Huang, H.-Y. Liao, Y.-C. Shiang, Z.-H. Lin, Z. Yang, H.-T. Chang, *J. Mater. Chem.* **2009**, *19*, 755.
[32] H. Cao, Y. Xiao, Y. Lu, J. Yin, B. Li, S. Wu, X. Wu, *Nano Res.* **2010**, *3*, 863.
[33] Q. Xianga, J. Yua, P. K. Wong, *J. Colloid Interface Sci.* **2011**, *357*, 163.
[34] Q. Xiang, J. Yu, W. Wang, M. Jaroniec, *Chem. Commun.* **2011**, *47*, 6906.
[35] Y.-D. Chiou, Y.-J. Hsu, *Appl. Catal. B* **2011**, *105*, 211.
[36] A. Houas, H. Lachheb, M. Ksibi, E. Elaloui, C. Guillar, J. M. Herrmann, *Appl. Catal. B* **2001**, *31*, 145.
[37] T. Hirakawa, Y. Nosaka, *Langmuir* **2002**, *18*, 3247–3254.
[38] J. G. Yu, B. Wang, *Appl. Catal. B* **2010**, *94*, 295.
[39] A. Gupta, M. Maynes, S. Silver, *Appl. Environ. Microbiol.* **1998**, *64*, 5042.
[40] T. Chasteen, R. Bentley, *Chem. Rev.* **2003**, *103*, 1.
[41] D. E. Taylor, *Trends Microbiol.* **1999**, *7*, 111.
[42] I. L. Calderón, F. A. Arenas, J. M. Pérez, D. E. Fuentes, M. A. Araya, C. P. Saavedra, J. C. Tantaleán, S. E. Pichuantes, P. A. Youderian, C. C. Vásquez, *PLoS ONE* **2006**, *1*, e70.
[43] A. Simon-Deckers, S. Loo, M. Mayne-L'hermite, N. Herlin-Boime, N. Menguy, C. Reynaud, B. Gouget, M. Carrière, *Environ. Sci. Technol.* **2009**, *43*, 8423.
[44] M. Li, L. Zhu, D. Lin, *Environ. Sci. Technol.* **2011**, *45*, 1977.
[45] R. Costi, G. Cohen, A. Salant, E. Rabani, U. Banin, *Nano Lett.* **2009**, *9*, 2031.
[46] J. Yu, J. Xiong, B. Cheng, S. Liu, *Appl. Catal. B* **2005**, *60*, 211.
[47] Z. Xu, J. Yu, G. Liu, *Electrochem. Commun.* **2011**, *13*, 1260.
[48] J. Yu, G. Dai, B. Huang, *J. Phys. Chem. C* **2009**, *113*, 16394.

Received: April 25, 2012
Revised: June 16, 2012

Nanomaterials

*Z.-H. Lin, Z.-Y. Shih, P. Roy, H.-T. Chang** .... ▮▮▮▮–▮▮▮▮

Preparation of Photocatalytic Au–Ag$_2$Te Nanomaterials

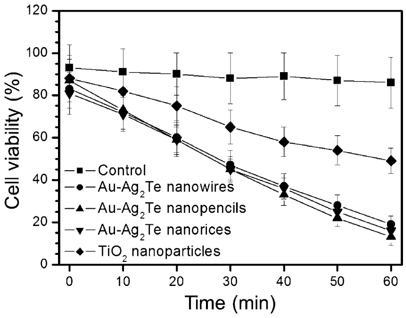

Au–Ag$_2$Te nanowires, nanopencils, and nanorice, which were prepared from the corresponding Ag$_2$Te nanomaterials by sequential spontaneous redox reactions with Au^{3+} and Ag^{+} ions under light irradiation at a concentration of 10 μg mL^{-1}, all provide a death rate of *Escherichia coli* greater than 80 % within 60 min. This is higher than the 51 % death rate for 100 μg mL^{-1} of commercial TiO$_2$ nanoparticles (see figure).